A novel LDMOS with a junction field plate and a partial N-buried layer*

Shi Xian-Long(石先龙)[a], Luo Xiao-Rong(罗小蓉)[a)b)†], Wei Jie(魏 杰)[a], Tan Qiao(谭 桥)[a], Liu Jian-Ping(刘建平)[a], Xu Qing(徐 青)[a], Li Peng-Cheng(李鹏程)[a], Tian Rui-Chao(田瑞超)[a], and Ma Da(马 达)[a]

[a] *State Key Laboratory of Electronic Thin Films and Integrated Devices. University of Electronic Science and Technology of China, Chengdu* 610054, *China*
[b] *Science and Technology on Analog Integrated Circuit Laboratory, Chongqing* 400060, *China*

(Received 30 June 2014; revised manuscript received 7 August 2014; published online 20 October 2014)

A novel lateral double-diffused metal–oxide semiconductor (LDMOS) with a high breakdown voltage (BV) and low specific on-resistance ($R_{on.sp}$) is proposed and investigated by simulation. It features a junction field plate (JFP) over the drift region and a partial N-buried layer (PNB) in the P-substrate. The JFP not only smoothes the surface electric field (E-field), but also brings in charge compensation between the JFP and the N-drift region, which increases the doping concentration of the N-drift region. The PNB reshapes the equipotential contours, and thus reduces the E-field peak on the drain side and increases that on the source side. Moreover, the PNB extends the depletion width in the substrate by introducing an additional vertical diode, resulting in a significant improvement on the vertical BV. Compared with the conventional LDMOS with the same dimensional parameters, the novel LDMOS has an increase in BV value by 67.4%, and a reduction in $R_{on.sp}$ by 45.7% simultaneously.

Keywords: junction field plate, partial N-buried layer, specific on-resistance, breakdown voltage

PACS: 73.40.Qv, 85.30.De, 85.30.Tv **DOI:** 10.1088/1674-1056/23/12/127303

1. Introduction

A lateral double-diffused metal–oxide–semiconductor field effect transistor (LDMOSFET) is widely used in smart power integrated circuits for its easy integration. The trade-off relationship between the breakdown voltage (BV) and the $R_{on.sp}$[1,2] is one of the main concerns of the LDMOSFET. The field plate (FP), reduced surface field (RESURF), reduced bulk field (REBULF), and varied lateral doping (VLD) have been widely used to improve the trade-off relationship. The conventional metal field plate (MFP) is easy to fabricate, but the E-field peak at the end of the MFP is prone to causing premature breakdown.[3,4] The resistive field plate (RFP) is a good choice to modulate the surface field distribution and improve the BV, however it brings a large intrinsic leakage current.[5] The RESURF technology can improve the BV and reduce the $R_{on.sp}$ simultaneously, but the P-top or P-buried layer (i.e. double /triple RESURF) narrows the current path in the N-drift region and induces a JFET region in the on-state, and thus restricts the decrease of the $R_{on.sp}$.[6–9] The REBULF technology enhances BV by introducing an N-type buried layer in the P-substrate to redistribute the E-field on the source side and the drain side.[10–12] Though the VLD in the drift region can achieve a high BV, the low doping on the source side leads to a 'hotspot'[13–15] and easily causes a thermal breakdown.

In this paper, a novel LDMOS with a junction field plate (JFP) over the drift region and a partial N-buried layer (PNB) in the P-substrate (JFP-PNB LDMOS) is proposed, which not only achieves a high breakdown voltage, but also realizes a very low specific on-resistance. The JFP results in a high doping concentration in the N-drift region by the charge compensation between the N-drift and the P region of the JFP. Furthermore, the linearly doped P region of the JFP modulates the surface E-field distribution, thus improving the BV and avoids the 'hotspot' in the drift region mentioned above. Moreover, the PNB is used to modulate the E-field distribution, and further improves the BV. The MEDICI simulator is used to study the mechanism of the JFP-PNB LDMOS. Simulated results demonstrate that the proposed JFP-PNB LDMOS has a good static performance.

2. Device structure and mechanism

Figure 1 shows the schematic cross section of the JFP-PNB LDMOS. The novel LDMOS features a PNB in the P-substrate and a PN^+ JFP on the field oxide. In the figure, L_p and T_{JFP} are the length and the thickness of the P region of the JFP, respectively; N_b and L_{nb} are the doping concentration and length of the PNB, respectively; T_w is the distance from the bottom surface of the drift region to the top of the N-buried layer. In addition, there is a P-type buried layer below the drift region at the source side; L_{bp} and N_{bp} are the length and the

*Project supported by the National Natural Science Foundation of China (Grant No. 61376079), the Program for New Century Excellent Talents in University of Ministry of Education of China (Grant No. NCET-11-0062), and the Postdoctoral Science Foundation of China (Grant Nos. 2012T50771 and XM2012004).

†Corresponding author. E-mail: xrluo@uestc.edu.cn

© 2014 Chinese Physical Society and IOP Publishing Ltd

doping concentration of the P-buried layer, respectively; N_d and T_d are the doping concentration and the thickness of the N-drift region, respectively.

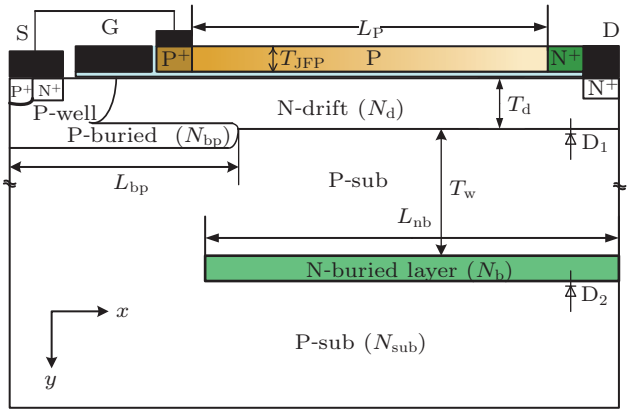


Fig. 1. (color online) Schematic cross section of the JFP-PNB LDMOSFET

In simulation, the physical models of CONSRH, AUGER, BGN, FLDMOB, IMPACT.I, and CCSMOB are mainly used, and the NEWTON solution method is carried out with 2 types of carriers and parameters of ITLIMIT = 30 and STACK = 15. The same dimensional parameters for several structures are set as follows: $L_p = 45$ μm, $T_{JFP} = 0.3$ μm, $L_{bp} = 21$ μm, $N_{bp} = 6 \times 10^{15}$ cm^{-3}, $T_d = 2$ μm, $N_{sub} = 2.5 \times 10^{14}$ cm^{-3}, and the half-cell pitch is 52 μm.

Figure 2 shows the equipotential contours of the JFP-PNB, PNB (without JFP), JFP (without PNB), and conventional LDMOSFETs at their own breakdown. As shown in Figs. 2(a) and 2(b), the PNB reshapes the equipotential contours, and thus uniform equipotential contours are formed in the bulk. However, for the JFP LDMOS and the conventional LDMOS in Figs. 2(c) and 2(d), without the PNB, the equipotential contours distribute intensively on the drain side, where the premature breakdown is prone to occur and voltage sustained by the source side is small. Furthermore, the additional reversed biased diode D_2 in Fig. 1 improves the vertical BV by extending the depletion depth. The fully depleted P-region of the JFP forms a charge compensation with the N-drift region in the off-state, which allows a much higher drift region doping at no expense of the BV. At the same time, the linearly doped P-region of the JFP can smooth the surface E-field distribution, which acts as a resistive field plate. Therefore, both the BV and the $R_{on.sp}$ are improved.

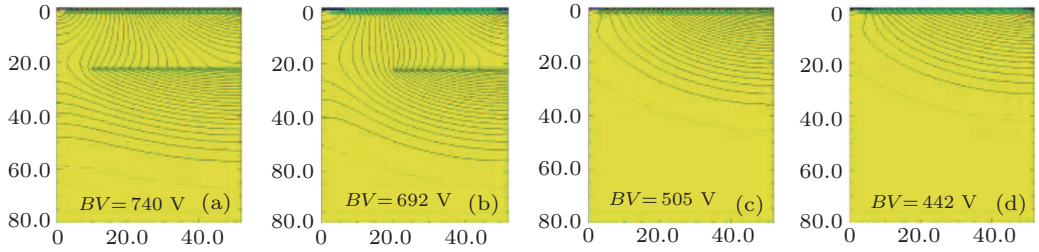


Fig. 2. (color online) Equipotential contours at breakdown for (a) JFP-PNB LDMOS (740 V), (b) PNB LDMOS (692 V), (c) JFP LDMOS (505 V), (d) conventional LDMOS (442 V) (20 V/contour).

3. Results and discussion

Figure 3 shows the E-field distribution at breakdown for the four devices mentioned above. In Fig. 3(a), the high y-component of the surface E-field demonstrates the assisted-depletion effect and charge compensation effect of the P region of the JFP on the N-drift region. The almost linear E-field distribution along the x-direction comes from the VLD in the JFP as shown by the image in the inset, and N_{base} and G are the background doping concentration and the doping gradient in the P region of the JFP, respectively.

Figure 3(b) provides the x-components of the surface E-field in the drift region. The E-field peaks exist at the end of the MFP for the conventional and PNB LDMOSFETs, leading to premature breakdown. In comparison, for the JFP-PNB and JFP LDOMSFETs, the JFP structure not only makes the E-field distribution much smoother, but also renders the average E-field higher. The linearly doped JFP works as if the RFP modulates the surface E-field, while the PN$^+$ junction in the JFP avoids the large leakage current in the off-state. On the other hand, the P-buried layer can improve the E-field on the source side, and introduces another E-field peak at its end, thus the BV further increases.

Figure 3(c) displays the lateral E-field distributions at $y = 10$ μm. They indicate that the high E-fields sharply decrease to zero from the drain side to the source side for the conventional and JFP LDMOSFETS. The high E-field concentrates on the drain side, where the breakdown can easily happen. However, for the JFP-PNB and PNB LDMOSFETs, the modulation effect of the PNB structure reduces the E-field peak and makes the E-field distribution more uniform, avoiding premature breakdown and improving the BV.

The vertical E-field distribution on the drain side is shown in Fig. 3(d). In the off-state, the PNB introduces an additional reverse biased diode D_2 (Fig. 1). For the PNB and JFP-PNB LDMOSFETs, the diode supports part of the vertical voltage drop and raises the vertical E-field strength in the P-substrate by extending the depletion region, which improves the vertical breakdown voltage.

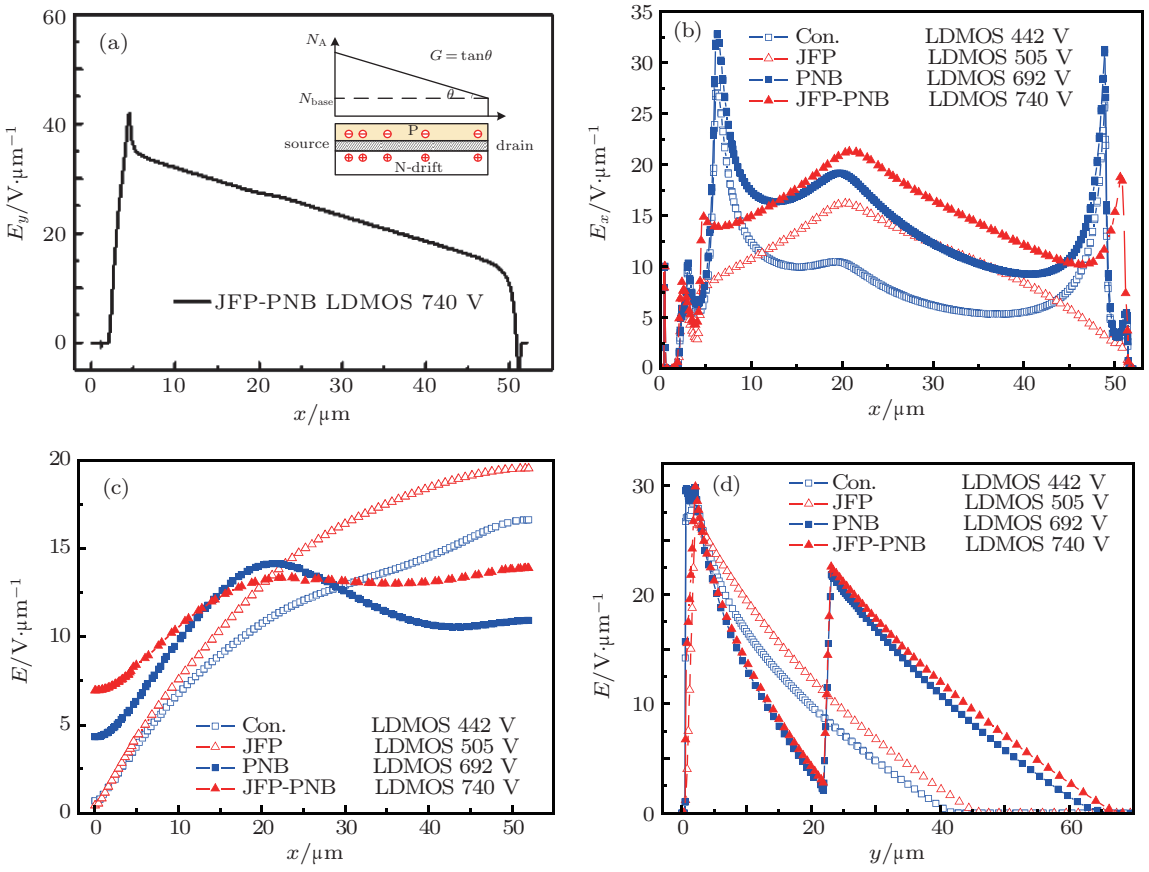


Fig. 3. (color online) E-field distributions for (a) y-component and (b) x-component of the surface E-field; (c) in the bulk ($y = 10$ μm); (d) vertical E-field at the end of the drain side. The inset in panel (a) illustrates the linear doping profile of the P region in the JFP.

Table 1. Comparison of the BV, N_d, $R_{on.sp}$, and FOM ($BV^2/R_{on.sp}$) among the four structures

Structure	$N_d/10^{15}$cm^{-3}	BV/V	$R_{on.sp}$/mΩ·cm^2	FOM/MW·cm^{-2}
JFP-PNB	12	740	67.3	8.1
PNB	4	692	166.3	2.9
JFP	13	505	62.9	4.1
Conventional	5.5	442	123.9	1.6

Owing to the charge compensation between the N-drift region and the P region of the JFP, the JFP-PNB and the JFP LDMOSFETs allow a much higher optimized N_d, as shown in Table 1. However, the optimized N_d of the JFP-PNB (or PNB) LDMOS is slightly lower than that of the JFP (or conventional) LDMOS, owing to the fact that the PNB supplies part of the N-type impurity in the off-state. Figure 4 shows the on-state current densities in the y direction at $x = 26$ μm for the four devices. The current densities of the JFP-PNB and JFP LDMOSFETs are more than twice those in the PNB and conventional LDMOSFETs. The JFP-PNB LDMOS reaches 740 V in BV and 67.3 mΩ·cm^2 in $R_{on.sp}$, which breaks the silicon limit of the triple RESURF LDMOS ($R_{on.sp}(\Omega\cdot\text{cm}^2) = 5.93\times10^{-9}\times32\times BV^2$).[2]

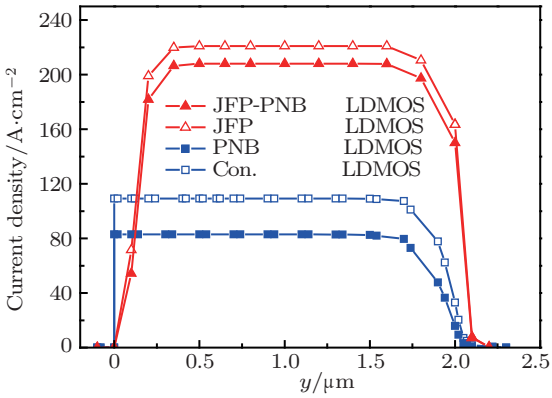


Fig. 4. (color online) On-state current densities at $x = 26$ μm varying with position in the y direction

Figure 5 indicates the influence of the length of the N-buried layer (L_{nb}) on BV and the voltage drop sustained by the D_1 and D_2 (V_{D1} and V_{D2}). The parameters are set as follows: $N_b = 1.6\times10^{16}$ cm^{-3}, $T_w = 30$ μm, $N_d = 1.2\times10^{16}$ cm^{-3}, $G = 1\times10^{19}$ cm^{-4}, and $N_{base} = 2.3\times10^{16}$ cm^{-3}. When $L_{nb} < 32$ μm, the BV keeps increasing with the increase of L_{nb}, but the BV begins to decrease at $L_{nb} = 32$ μm. The variations of V_{D1} and V_{D2} determine the change of the BV. When $L_{nb} < 32$ μm, the N-drift region is fully depleted at breakdown, V_{D1} keeps nearly constant, and the V_{D2} increases due to the extension of the depletion depth, therefore the increase of the BV

is totally determined by raising V_{D2}. When $L_{nb} > 32$ μm, the drift region becomes un-depleted, then the V_{D1} decreases with the increase of L_{nb}, V_{D2} is limited by the premature breakdown at the drift region surface on the source side, and the decrease of the BV is determined by reducing V_{D1}.

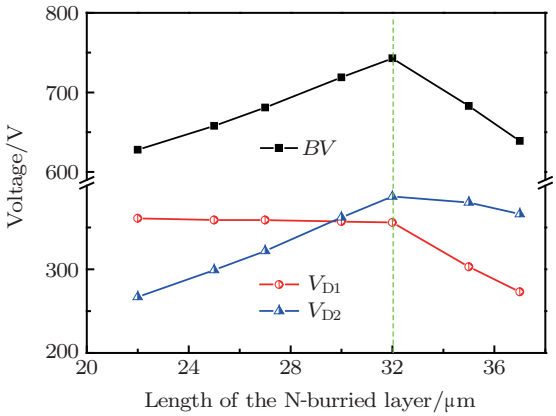


Fig. 5. (color online) Dependences of BV, V_{D1}, and V_{D2} on the length of the N-buried layer. The V_{D1} and V_{D2} represent the voltage shared by the diodes D_1 and D_2 respectively.

Figure 6 demonstrates the vertical potential (a) and E-field (b) distributions at the drain end for the T_w values of 10, 20, and 35 μm respectively. The vertical arrows with dash line arrows in panel (a) refer to the potential drop on the diode D_1 (V_{D1}), and the solid ones represent V_{D2}. With the increase of T_w, V_{D1} keeps increasing and V_{D2} keeps decreasing. If T_w is too small, the voltage sustained by D_1 decreases. The case will be the same for D_2 if T_w is too large. These two conditions both degrade the BV. According to the simulation by MEDICI, the optimized T_w value is in a range of 15 μm–30 μm.

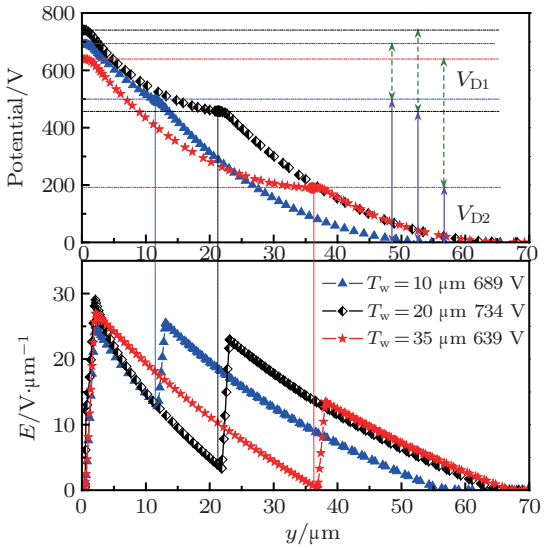


Fig. 6. (color online) Vertical potential and E-field distributions at the end of the drain side for different values of T_w.

Figure 7 shows the influences of the G on the BV and N_{base}, with $N_b = 1.3 \times 10^{16}$, 1.9×10^{16}, and 2.2×10^{16} cm^{-3} respectively. The charge balance is shown in the following equations:

$$Q^+_{N-drift} + Q^+_{N-buried} = Q^-_{JFP} + Q^-_{P-sub}, \quad (1)$$

$$Q^-_{JFP} = (N_{base} + 0.5 \cdot G \cdot L_P) \cdot T_{JFP}. \quad (2)$$

Owing to the charge balance, the optimized N_{base} will decrease if the G increases for the same value of N_b. At the same time, for a given G, N_{base} increases with the increase of N_b. Though the N_{base} and the N_b can be matched in a large range, there is an optimum N_b. In Fig. 7, the BV is at its highest at $N_b = 1.9 \times 10^{16}$ cm^{-3}.

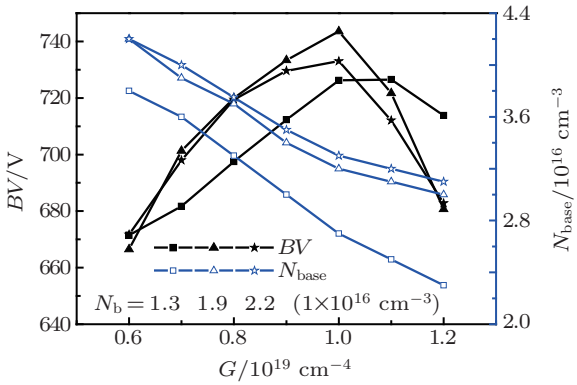


Fig. 7. (color online) Dependences of BV and N_{base} on G each as a function of N_b

Figure 8 shows the influences of the N_d on the BV for the four different LDMOSFETs. All of the data are optimized for each device. First, the optimized N_d values of the LDMOSFETs with JFP are much higher than those of the devices without JFP. Second, the LDMOSFETs with the JFP can be optimized in a much wider range of N_d, which provides flexible designs for the engineers for different conditions. Third, the BV of the LDMOSFETs with the PNB is much higher.

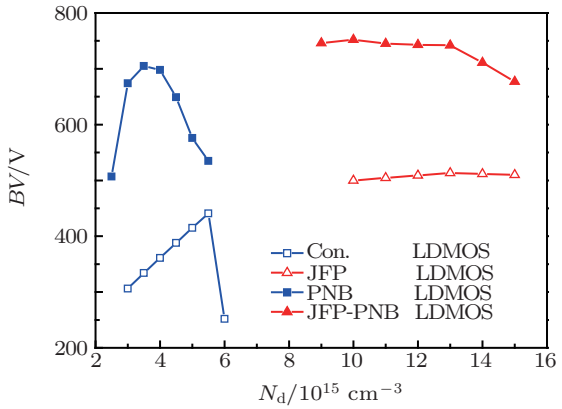


Fig. 8. (color online) Dependences of BV on N_d for the four devices

Figure 9 shows the key fabrication steps of the JFP-PNB LDMOS. In step (a) the impurity source is the arsenic, and the low diffusion coefficient of the arsenic can ensure the PNB keeps its shape well after the process of epitaxy. Steps (e)–(g)

show the process of the impurity implantation and annealing, including P^+ contact, P^+ anode region, N^+ source, N^+ drain, N^+ cathode region, and the linearly doped P region of the JFP. The linear doping can be achieved with only one mask by controlling the sizes and the spaces of the mask windows, which is shown in step (g).[14,15]

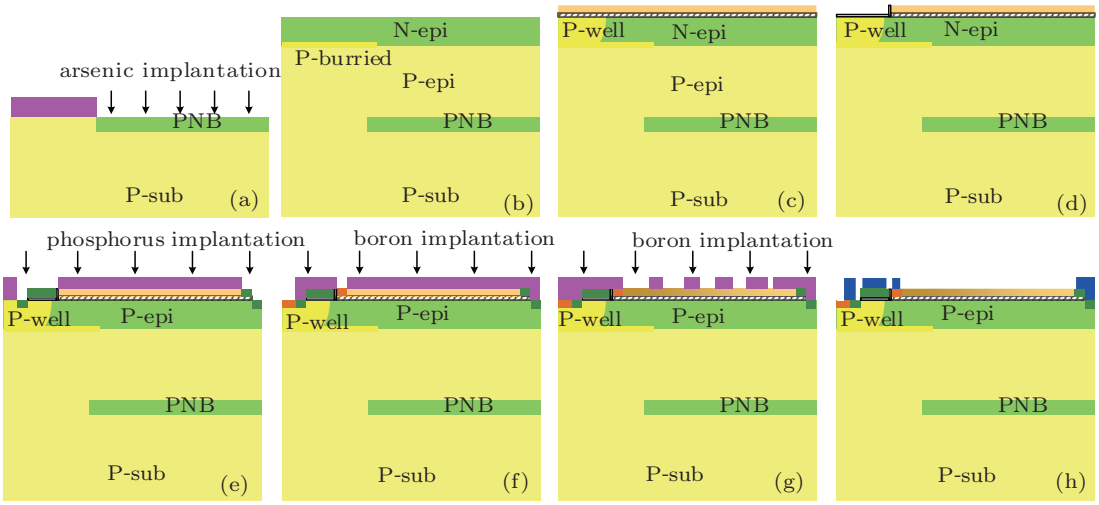


Fig. 9. (color online) Key process steps of the JFP-PNB LDMOS for forming (a) PNB; (b) an epitaxial layer; (c) P-well and the JFP film; (d) gate oxide and the isolator between the gate and the JFP; (e)–(g) impurity implantation and annealing; and (h) electrodes.

4. Conclusion

A novel LDMOS equipped with a JFP and a PNB is proposed and investigated by simulation. In the off-state, the JFP brings in a charge compensation effect on the N-drift region and smoothes the surface E-field. At the same time, the PNB reduces the E-field peak on the drain side and increases the E-field strength on the source side, and the additional vertical diode extends the vertical depleted area in the substrate. All effects improve the BV and $R_{\text{on.sp}}$. Simulation demonstrates that the BV of 740 V and the $R_{\text{on.sp}}$ of 67.3 m$\Omega\cdot$cm^2 are obtained for the proposed JFP-PNB LDMOS at 52-μm half-cell pitch. Compared with the conventional LDMOS, the proposed one increases the BV by 67.4% and reduces the $R_{\text{on.sp}}$ by 45.7% simultaneously. The proposed structure obtains a superior trade-off relationship between the BV and $R_{\text{on.sp}}$, which is far better than that for the triple-RESURF LDMOS.

References

[1] Ludikhuize A W 2001 *IEEE Solid-State Device Research Conference*, September 11–13, 2001, *Proceeding of the* 31*st European*, p. 35

[2] Iqbal M M, Udrea F and Napoli E 2009 *IEEE Proceedings of the* 21*st International Symposium on Power Semiconductor Devices and ICs*, June 14–18, 2009, Barcelona, Spain, p. 247

[3] Lee M R and Kwon O K 1999 *IEEE Proceedings of the* 11*th International Symposium on Power Semiconductor Devices and ICs*, May 26–28, 1999, Toronto, Canada, p. 249

[4] Xie G, Xu E, Hashemi N, Zhang B, Fu F Y and Wai T N 2012 *Chin. Phys. B* **21** 086105

[5] Yahata A and Atsuta M 1995 *IEEE Proceedings of the* 7*th International Symposium on Power Semiconductor Devices and ICs*, May 23–25, 1995, Yokohama, Japan, p. 400

[6] Ludikhuize A W 2000 *IEEE Proceedings of the* 12*th International Symposium on Power Semiconductor Devices and ICs*, May 22–25, 2000, Toulouse, France, p. 11

[7] Luo X R, Yao G L, Zhang Z Y, Jiang Y H, Zhou K, Wang P, Wang Y G, Lei T F, Zhang Y X and Wei J 2012 *Chin. Phys. B* **21** 068501

[8] Luo X R, Luo Y C, Fan Y, Hu G Y, Wang X W, Zhang Z Y, Fan Y H, Cai J Y, Wang P and Zhou K 2013 *Chin. Phys. B* **22** 027304

[9] Luo, X, Zhang B and Li Z 2007 *Solid-State Electronics* **51** 493

[10] Duan B X, Zhang B and Li Z J 2006 *IEEE International Conference on Communications, Circuits and Systems Proceedings*, June 25–28, 2006, Guilin, China, Vol. **4**, p. 2709

[11] Zhang B, Duan B X and Li Z J 2006 *J. Semicond.* **27** 4

[12] Cheng J B, Zhang B and Li Z J 2008 *IEEE Electron Dev. Lett.* **29** 645

[13] Leung Y K, Paul A K, Goodson K E, Plummer J D and Wong S 1997 *IEEE Electron Dev. Lett.* **18** 414

[14] Zhang S D, Sin K O, Lai T M L and Ko P K 1999 *IEEE Trans. Electron Dev.* **46** 1036

[15] Jiang H, Zhang B, Chen W, Li Z, Zheng C, Liu C, Rao Z and Dong B 2012 *IEEE Proceedings of the* 24*th International Symposium on Power Semiconductor Devices and ICs*, June 3–7, 2012, Bruges, Belgium, p. 173